

# Electron Beam Supercollimation in Graphene Superlattices

Cheol-Hwan Park<sup>1,2</sup>, Young-Woo Son<sup>3,4</sup>, Li Yang<sup>1,2</sup>, Marvin L. Cohen<sup>1,2</sup>, and Steven G. Louie<sup>1,2\*</sup>

<sup>1</sup>*Department of Physics, University of California at Berkeley, Berkeley, California 94720 USA*

<sup>2</sup>*Materials Sciences Division, Lawrence Berkeley National Laboratory, Berkeley, California 94720 USA*

<sup>3</sup>*Department of Physics, Konkuk University, Seoul 143-701, Korea*

<sup>4</sup>*School of computational sciences, Korea institute for advanced study, Seoul 130-722, Korea*

(Dated: August 23, 2008)

Although electrons and photons are intrinsically different, importing useful concepts in optics to electronics performing similar functions has been actively pursued over the last two decades. In particular, collimation of an electron beam is a long-standing goal. We show that ballistic propagation of an electron beam with virtual no spatial spreading or diffraction, without a waveguide or external magnetic field, can be achieved in graphene under an appropriate class of experimentally feasible one-dimensional external periodic potentials. The novel chiral quasi-one-dimensional metallic state that the charge carriers are in originates from a collapse of the intrinsic helical nature of the charge carriers in graphene owing to the superlattice potential. Beyond providing a new way to constructing chiral one-dimensional states in two dimensions, our findings should be useful in graphene-based electronic devices (e. g., for information processing) utilizing some of the highly developed concepts in optics.

Electronic analogues of many optical behaviors such as focusing [1, 2, 3], collimation [4], and interference [5] have been achieved in two-dimensional electron gas (2DEG), enabling the system as a basic platform to study fundamental problems in quantum mechanics [6, 7, 8] as well as quantum information processing [9]. The close relationship between optics and electronics is been made possible due to the ballistic transport properties of a high-mobility 2DEG created in semiconductor heterostructures [10]. Among those electronics-optics analogues, the collimation or quasi-one-dimensional (quasi-1D) motion of electrons and photons are particularly important not only to achieve electronic quantum devices [7, 9] but also to realize ultracompact integrated light circuits [11, 12]. Usually, electrons originated from a point source may be controlled by electrostatics or geometrical constrictions [2, 3]. Quasi-1D electronic states and focusing have been achieved in a 2DEG with the help of external magnetic fields, e. g., employing magnetic focusing [1] and quantum Hall edge states [7, 13]. However, it would be difficult to integrate them into a single electronic device due to the external high magnetic field apparatus needed. In view of recent successful demonstrations of extreme anisotropic light propagation without diffraction, called supercollimation in photonic crystals [11, 12, 14, 15], an analogue of this effect in two-dimensional (2D) electron systems may also be possible. In this work, we demonstrate that graphene [16, 17, 18] in an external periodic potentials, or a graphene superlattice, is particularly suitable to realize electron supercollimation in two dimensions.

The isolation of graphene [16, 17, 18], a single layer of carbon atoms in a honeycomb structure composed of two equivalent sublattices, offers a new dimension to study electronics-optics analogues. Carriers in graphene exhibit ballistic transport on the submicron scale at room temperature [19] and with mobility up to  $2 \times$

$10^5 \text{ cm}^2 \text{ V}^{-1} \text{ s}^{-1}$  [20]. Graphene electronic states have an internal quantum number, a pseudospin, that is not found in normal electronic systems and strongly influences the dynamics of the charge carriers. The pseudospin is of central importance to many of the novel physical properties of graphene [16, 17, 18, 19, 20, 21, 22], and it also plays a significant role in the present work.

The low-energy quasiparticles in graphene whose wavevectors are close to the Dirac point  $\mathbf{K}$  in the Brillouin zone are described by a  $2 \times 2$  Hamiltonian matrix  $H_0(\mathbf{k}) = \hbar v_0 (\sigma_x k_x + \sigma_y k_y)$ , where  $v_0 \approx 10^6 \text{ m/s}$  is the band velocity,  $\mathbf{k}$  is the wavevector measured from the  $\mathbf{K}$  point, and  $\sigma$ 's are the Pauli matrices. The energy eigenvalues are given by  $E_s^0(\mathbf{k}) = s \hbar v_0 |\mathbf{k}|$  where  $s = +1 (-1)$  denotes the conical conduction (valence) band (Fig. 1B). The sublattice degree of freedom of the quasiparticles in graphene can conveniently be described with a pseudospin basis, or spinors, where the  $|\uparrow\rangle$  and the  $|\downarrow\rangle$  pseudospin states of  $\sigma_z$  represent  $\pi$ -electron orbital on the  $A$  and  $B$  sublattices of the structure of graphene, respectively. This Hamiltonian is very similar to the one used to model neutrinos as massless Dirac fermions [23, 24]. The corresponding wavefunction is given by

$$\psi_{s,\mathbf{k}}^0(\mathbf{r}) = \frac{1}{\sqrt{2}} \begin{pmatrix} 1 \\ s e^{i\theta_{\mathbf{k}}} \end{pmatrix} e^{i\mathbf{k} \cdot \mathbf{r}}, \quad (1)$$

where  $\theta_{\mathbf{k}}$  is the angle of the wavevector  $\mathbf{k}$  with respect to the  $x$ -axis. Equation (1) may be viewed as having the pseudospin vector being parallel and antiparallel to the wavevector  $\mathbf{k}$  for electronic states in the upper ( $s = 1$ ) and the lower ( $s = -1$ ) band, respectively (Fig. 1B) [23, 24]. As the spin plays a role in the dynamics of neutrinos, the present pseudospin is similarly important in the quasiparticle dynamics of graphene [23, 24].

Now, let us consider a 1D external periodic potential  $V(x)$  applied to graphene. The potential is taken to vary

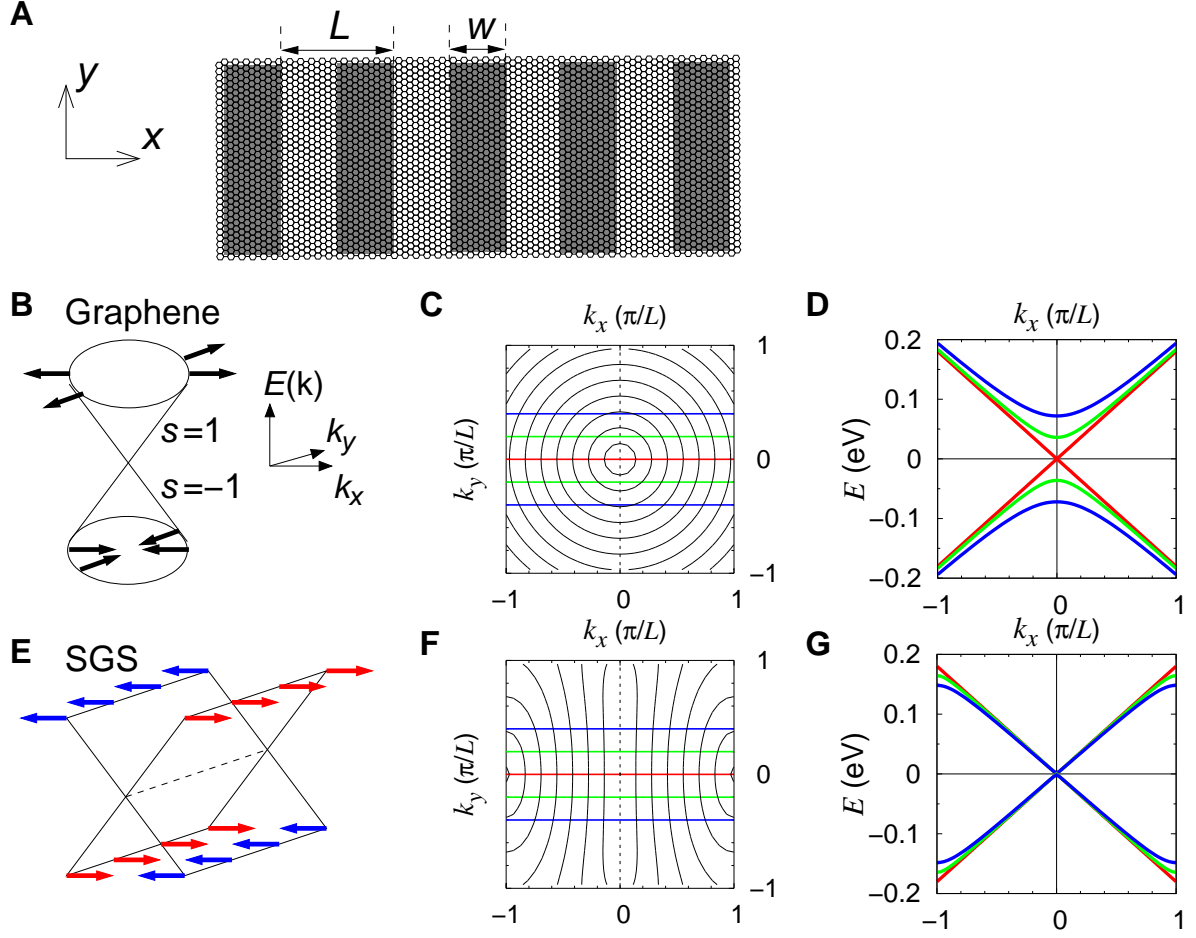


FIG. 1: Electron energy dispersion relation in a special graphene superlattice. (A) Schematic diagram of a Kronig-Penney type of potential applied to graphene with strength  $U_0$  inside the gray regions and zero outside. The lattice period is  $L$  and the barrier width is  $w$ . (B) Schematic diagram showing the electronic energy dispersion relations and pseudospin vectors (black arrows) in graphene. (C) Contour plot of the first electronic band above the Dirac point energy in pristine graphene. The energy difference between neighbouring contours is 25 meV, with the lowest contour near the origin having a value of 25 meV. (D) The electronic energy dispersion relation  $E$  versus  $k_x$  with fixed  $k_y$ . Red, green and blue lines correspond to  $k_y = 0$ ,  $0.1 \pi/L$  and  $0.2 \pi/L$ , respectively, as indicated in C. (E), (F) and (G) Same quantities as in B, C and D for the considered SGS ( $U_0 = 0.72$  eV,  $L = 10$  nm and  $w = 5$  nm). Red and blue arrows in E represent the ‘right’ and the ‘left’ pseudospin state, respectively.

much more slowly than the carbon-carbon distance so that inter-valley scattering can be neglected [23, 24]. Under this condition and for low-energy quasiparticle states whose wavevectors are close to the  $\mathbf{K}$  point, the Hamiltonian reads

$$H = \hbar v_0 (-i\sigma_x \partial_x + \sigma_y k_y + I V(x)/\hbar v_0), \quad (2)$$

where  $I$  is the  $2 \times 2$  identity matrix. The eigenstates and eigenenergies of the Hamiltonian  $H$  in Eq. (2) may be obtained numerically in the general case or analytically for small  $\mathbf{k}$ .

It has been predicted that, in a graphene superlattice with a slowly varying 1D periodic potential or a 2D periodic potential of rectangular symmetry, the group velocity of its low-energy charge carriers is renormalized anisotropically [25]. Unlike bare graphene which

has an isotropic (zero mass) relativistic energy dispersion (Figs. 1B, 1C and 1D), graphene under some specific superlattice potentials displays extremely anisotropic quasiparticle energy dispersion: the group velocity near the Dirac point along the direction perpendicular to the periodicity of the potential vanishes while the one parallel to the periodicity direction is intact [25].

We consider a Kronig-Penney type of potential with barrier height  $U_0$ , lattice period  $L$ , and barrier width  $w$ , periodic along the  $x$  direction (Fig. 1A). These potential parameters can be tuned so that the group velocity of the quasiparticles (with wavevector close to the Dirac point) along the  $y$  direction vanishes [25]. We shall focus on a graphene superlattice under one of these conditions ( $U_0 = 0.72$  eV,  $L = 10$  nm, and  $w = 5$  nm) [25]. The parameters used here are experimentally feasible as shown

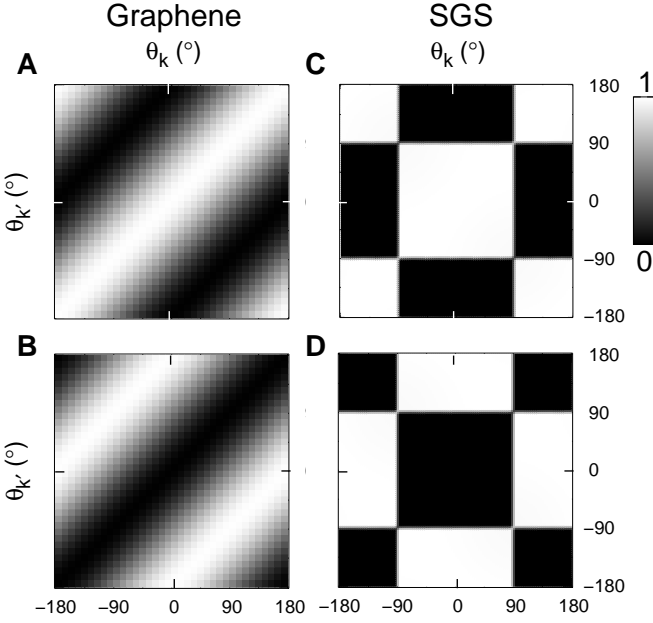


FIG. 2: Pseudospin collapse in a special graphene superlattice. (A) and (B) Calculated overlap of two quasiparticle states  $\psi_{s,\mathbf{k}}^0(\mathbf{r})$  and  $\psi_{s',\mathbf{k}'}^0(\mathbf{r})$ ,  $\left| \left\langle \psi_{s',\mathbf{k}'}^0 | e^{i(\mathbf{k}'-\mathbf{k})\cdot\mathbf{r}} | \psi_{s,\mathbf{k}}^0 \right\rangle \right|^2$ , in graphene versus  $\theta_{\mathbf{k}}$  and  $\theta_{\mathbf{k}'}$  which are the angles between the  $x$  axis and wavevectors  $\mathbf{k}$  and  $\mathbf{k}'$  ( $|\mathbf{k}| = |\mathbf{k}'| = 0.1\pi/L$ ), respectively. The overlap is shown in a gray scale (0 in black and 1 in white). The two states are in the same band ( $s' = s$ ) in A and are in different bands ( $s' = -s$ ) in B. (C) and (D) Same quantities as in A and B for the considered SGS ( $U_0 = 0.72$  eV,  $L = 10$  nm and  $w = 5$  nm).

in recent studies [26, 27, 28, 29]. Later, we will relax the special condition to confirm the robustness of the predicted supercollimation.

The quasiparticle energy dispersion of this superlattice (Figs. 1E, 1F and 1G) shows that, not only the group velocity of quasiparticles at the Dirac point along the  $y$  direction vanishes, there is hardly any dispersion along the  $k_y$  direction within a good fraction of the supercell Brillouin zone (Figs. 1F and 1G). This portion of the energy dispersion in this superlattice thus is well described by the relation

$$E_s(\mathbf{k}) = s\hbar v_0 |k_x|. \quad (3)$$

The deviation of the actual energy dispersion from that of Eq. (3) is less than 5% for  $\mathbf{k}$  vector as large as 40% of the supercell Brillouin zone considered (Figs. 1F and 1G). This is an equation for wedges. Thus, for some specific superlattice potentials, graphene turns from a zero-gap semiconductor into a quasi-1D metal with a finite and constant density of states about the Dirac point energy. We shall call this class of graphene superlattices as special graphene superlattices (SGSs).

Along with the quasiparticle energy dispersion, the internal pseudospin symmetry of the electronic states in

SGSs also undergoes a dramatic alteration. We calculate numerically the overlap  $\left| \left\langle \psi_{s',\mathbf{k}'} | e^{i(\mathbf{k}'-\mathbf{k})\cdot\mathbf{r}} | \psi_{s,\mathbf{k}} \right\rangle \right|^2$  of two quasiparticle states  $\psi_{s,\mathbf{k}}(\mathbf{r})$  and  $\psi_{s',\mathbf{k}'}(\mathbf{r})$ . If there were no external periodic potential, this overlap would be simply  $(1 + ss' \cos(\theta_{\mathbf{k}'} - \theta_{\mathbf{k}}))/2$  as seen from Eq. (1) (Figs. 2A and 2B). The same overlap in the SGS (Figs. 2C and 2D) is however dramatically different from that in graphene, and can be well described by  $\left| \left\langle \psi_{s',\mathbf{k}'} | e^{i(\mathbf{k}'-\mathbf{k})\cdot\mathbf{r}} | \psi_{s,\mathbf{k}} \right\rangle \right|^2 = (1 + ss' \text{sgn}(k_x) \text{sgn}(k'_x))/2$ . This behavior is robust for a wide range of the magnitudes of  $\mathbf{k}$  and  $\mathbf{k}'$ , extending over a good fraction of the supercell Brillouin zone with a high degree of accuracy. The eigenfunctions of an SGS, for states with small  $\mathbf{k}$ , can be deduced from this result, together with results on the numerically obtained wavefunctions, (also from analytic calculation: see Supporting Information) as having the form of

$$\psi_{s,\mathbf{k}}(\mathbf{r}) = e^{if(x)} \frac{1}{\sqrt{2}} \begin{pmatrix} 1 \\ s \text{sgn}(k_x) \end{pmatrix} e^{i\mathbf{k}\cdot\mathbf{r}}, \quad (4)$$

where  $f(x)$  is a real function. Thus, the spinor in Eq. (4) is an eigenstate of  $\sigma_x$ . Therefore, the direction of the pseudospin is quantized so that it is either parallel or anti-parallel to the  $x$  direction, which is the direction of the periodicity of the superlattice potential (Fig. 1E), and not to the wavevector  $\mathbf{k}$  as is the case in pristine graphene (Fig. 1B). In other words, the pseudospin in the SGS collapses into a backward ('left') or a forward ('right') state. The resulting quasi-one-dimensionality in the energy dispersion relation and in the pseudospin of quasiparticles in the SGS significantly changes the already unique properties of graphene.

The quasi-one-dimensionality and specific chiral nature of the SGS makes it a natural candidate for electron supercollimation. It is indeed the case that, when a wavepacket of electron is injected into an SGS, the propagating packet exhibits essentially no spatial spreading, i.e., electron beam supercollimation is realized (Fig. 3). We have calculated the time-evolution of a gaussian wave packet (with spatial extent along the  $x$  and the  $y$  direction given by  $2\sigma_x = 40$  nm and  $2\sigma_y = 200$  nm, respectively) composed of states in the first band above the Dirac point energy with a central wavevector  $\mathbf{k}_c$  (Fig. 3). To provide a measure of the electron beam collimation, we compute the angle  $\theta_c$  in which direction the beam intensity is maximum and the angular spread  $\Delta\theta$  which gives half the maximum intensity when the angle is at  $\theta_c \pm \Delta\theta$ . For a central wavevector  $\mathbf{k}_c$  parallel to the  $x$  direction with energy  $E(\mathbf{k}_c) = E_0 = \hbar v_0 0.1\pi/L = 0.02$  eV, the angular spread  $\Delta\theta$  in pristine graphene is  $\Delta\theta = 55^\circ$  (Fig. 3A), whereas in the SGS,  $\Delta\theta = 0.3^\circ$  (Fig. 3B), about 200 times smaller than in graphene. Specifically, in the SGS, the spread of the wave packet in the  $y$  direction after proceeding 0.1 mm along the  $x$  direction is only 500 nm. Therefore, supercollimation of currents of

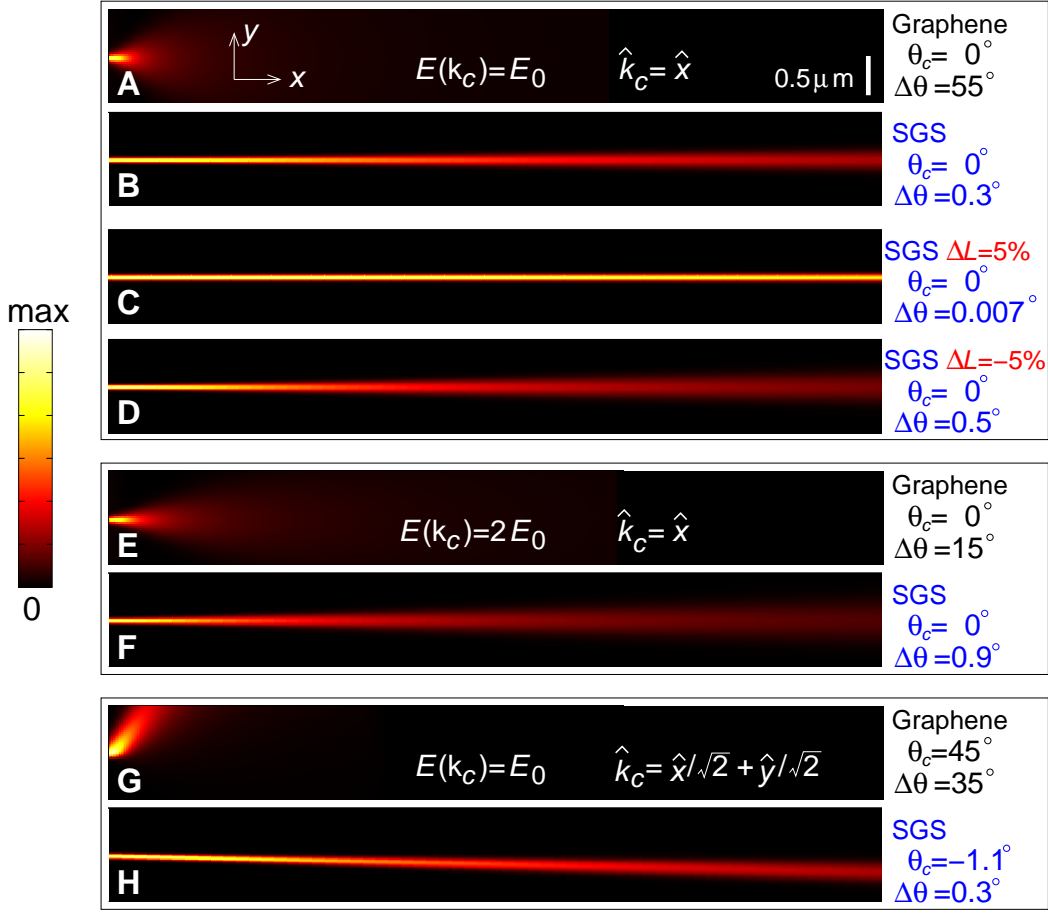


FIG. 3: Special graphene superlattice as an electron supercollimator. (A), (E) and (G) Time-integrated probability density of an electron wave packet,  $\int_0^\infty |\Psi(x, y, t)|^2 dt$ , in graphene. The initial ( $t = 0$ ) wave packet is a Gaussian localized at the coordinates origin (middle of the left edge of each panel)  $|\Psi(x, y, 0)|^2 \sim \exp[-(x^2/2\sigma_x^2 + y^2/2\sigma_y^2)]$  where  $2\sigma_x = 200$  nm and  $2\sigma_y = 40$  nm. The wave packet in wavevector space is set to be localized around a specific  $\mathbf{k}_c$ . In A,  $\mathbf{k}_c$  is set by  $E(\mathbf{k}_c) = E_0 = \hbar v_0 0.1\pi/L = 0.02$  eV and  $\hat{k}_c = \hat{x}$ . In E,  $\mathbf{k}_c$  is set by  $E(\mathbf{k}_c) = 2E_0$  and  $\hat{k}_c = \hat{x}$ . In G,  $\mathbf{k}_c$  is set by  $E(\mathbf{k}_c) = E_0$  and  $\hat{k}_c = \hat{x}/\sqrt{2} + \hat{y}/\sqrt{2}$ .  $\theta_c$  denotes the angle (defined with respect to the  $x$ -direction) along which direction the intensity is maximal and  $\Delta\theta$  denotes the angular spread which gives half the maximum intensity when the angle is at  $\theta_c \pm \Delta\theta$ . (B), (F) and (H) Same quantities as in A, E and G for the considered SGS ( $U_0 = 0.72$  eV,  $L = 10$  nm and  $w = 5$  nm), respectively. (C) and (D), Same quantities as in B for graphene superlattices corresponding to a superlattice potential that is otherwise the same as the SGS studied but with a period  $L$  change of  $\Delta L/L = 5\%$  and  $\Delta L/L = -5\%$ , respectively.

nanoscale width in the SGS can, in principle, be achieved and maintained as long as the ballistic transport occurs in the system.

Even when the experimental situation deviates from the ideal conditions for SGSs, supercollimation persists. Hence the phenomenon is quite robust. First, for example, if we consider an imperfection in making a superlattice potential such that the periodicity is slightly larger or smaller ( $\Delta L/L = \pm 5\%$ ), the calculated time-evolution of a gaussian wave packet shows the angular spread  $\Delta\theta = 0.007^\circ$  and  $0.5^\circ$ , respectively (Figs. 3C and 3D). Second, when considering doped SGSs or high energy electron injection such that  $E(\mathbf{k}_c)$  is doubled, the angular spread is still very small (Fig. 3F). Third, even when  $\mathbf{k}_c$  is off from the collimation direction ( $+x$ ) by

$45^\circ$ , the angular deviation is still negligible ( $\theta_c = -1.1^\circ$ ) (Fig. 3H). In graphene, on the other hand, the propagation direction and spread of the wave packet sensitively depends on the magnitude and the direction of the central wavevector  $\mathbf{k}_c$  (Figs. 3E and 3G). This robustness here is quite contrary to the case in optics where the efficiency of supercollimator, superprism or superlens [30] depends sensitively on the magnitude and the direction of the light wavevector and in general provides a very narrow effective bandwidth [11, 12, 14, 15]. From our calculations, we expect that the predicted supercollimation be observable in SGSs over a wide operation range.

Lastly, we consider the tunneling properties of injected electrons into SGSs from pristine graphene, which provides another measure of the efficiency of electronic de-

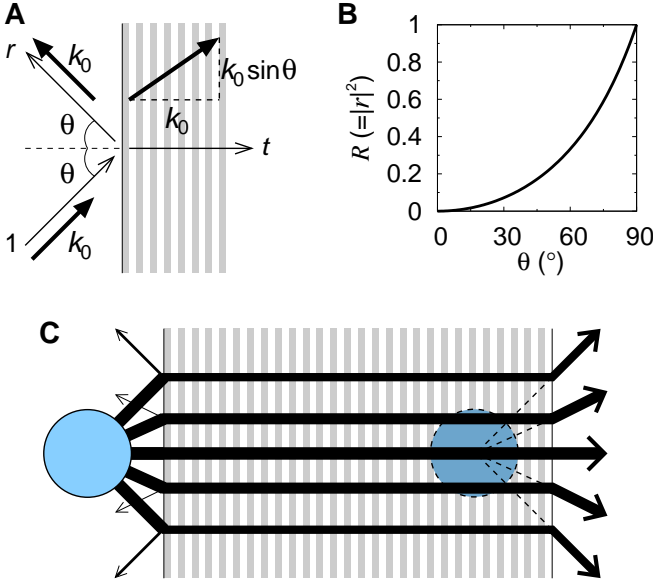


FIG. 4: Reflection and transmission at a graphene – special graphene superlattice interface and virtual imaging. (A) Schematic diagram showing the incident, the reflected and the transmitted wave (the band index is set to  $s = 1$ ) at a graphene – SGS interface, with the relative amplitudes being 1,  $r$  and  $t$ , respectively. Thick arrows represent the wavevectors of the corresponding waves. The incidence and reflection angle is  $\theta$ . (B) Reflectance  $R = |r|^2$  versus the incidence angle  $\theta$ . (C) Schematic diagram showing the propagation of electron waves in graphene – SGS – graphene geometry. Thickness of each arrow is proportional to the actual intensity of the wave. A virtual image (dashed disk) is formed at a place far from the actual wave source (solid disk).

vices based on SGSs. When an electron is injected into an SGS with an incidence angle  $\theta$  from the graphene side, the wavevector of incident electron is given by  $\mathbf{k}_i = k_0 \cos \theta \hat{x} + k_0 \sin \theta \hat{y}$  and those of the reflected and transmitted electrons by  $\mathbf{k}_r = -k_0 \cos \theta \hat{x} + k_0 \sin \theta \hat{y}$  and  $\mathbf{k}_t = k_0 \hat{x} + k_0 \sin \theta \hat{y}$ , respectively (Fig. 4A). Here, we have made use of the continuity of the transverse component of the wavevector and conservation of energy, together with the novel dispersion relation given by Eq. (3). Using the continuity of the wavefunction in the system described by Eqs. (1) and (4), we find that the reflectance  $R = |r|^2$  is

$$R(\theta) = \tan^2 \frac{\theta}{2}. \quad (5)$$

Interestingly, the reflectance is independent of the specific form of the external periodic potential of the SGS. Equation (5) indicates that the transmittance is large for most incidence angles. For example, even at  $\theta = 45^\circ$ , the reflectance is less than 20 % (Fig. 4B). Therefore, the SGS is not only an excellent electron supercollimator but also a good transmitter in a graphene-SGS-graphene junction (Fig. 4C). Utilizing this property, an immedi-

ate application could be made to demonstrate an electronic analogue of virtual imaging in this configuration (Fig. 4C).

Given the recent rapid progress in graphene superlattices fabrication [26, 27, 28, 29], the manipulation of electrons in ways similar to that of photons in optics by using the supercollimation effect discussed here together with other optics analogues [21, 22] is expected to soon be practicable. The SGSs have the promise of playing a unique role in devices based on the synergetic importing of concepts and techniques well developed in optics to electronics.

**Acknowledgement.** We thank D. S. Novikov and J. D. Sau for fruitful discussions. This research was supported by NSF grant DMR07-05941 and by DOE grant DE-AC02-05CH11231. Y.-W.S. was supported by KOSEF grant R01-2007-000-10654-0 and by Nano R&D program 2008-03670 through the KOSEF funded by the Korean government (MEST). Computational resources have been provided by NPACI and NERSC.

---

\* Electronic address: sglouie@berkeley.edu

- [1] H. van Houten, B. J. van Wees, J. E. Mooij, C. W. J. Beenakker, J. G. Williamson, and C. T. Foxon, *Europhys. Lett.* **5**, 721 (1988).
- [2] J. Spector, H. L. Stormer, K. W. Baldwin, L. N. Pfeiffer, and K. W. West, *Appl. Phys. Lett.* **56**, 1290 (1990).
- [3] U. Sivan, M. Haiblum, C. P. Umbach, and H. Shtrikman, *Phys. Rev. B* **41**, R7937 (1990).
- [4] L. W. Molenkamp, A. A. M. Staring, C. W. J. Beenakker, R. Eppenga, C. E. Timmering, J. G. Williamson, C. J. P. M. Harmans, and C. T. Foxon, *Phys. Rev. B* **41**, R1274 (1990).
- [5] A. Yacoby, M. Heiblum, V. Umansky, H. Shtrikman, and D. Mahalu, *Phys. Rev. Lett.* **73**, 3149 (1994).
- [6] E. Buks, R. Shuster, M. Heiblum, D. Mahalu, and V. Umansky, *Nature* **391**, 871 (1998).
- [7] Y. Ji, Y. Chung, D. Sprinzak, M. Heiblum, D. Mahalu, and H. Shtrikman, *Nature* **422**, 415 (2003).
- [8] D.-I. Chang, G. L. Khym, K. Kang, Y. Chung, H.-J. Lee, M. Seo, M. Heiblum, D. Mahalu, and V. Umansky, *Nature Phys.* **4**, 205 (2008).
- [9] C. W. J. Beenakker, C. Emary, M. Kindermann, and J. L. van Velsen, *Phys. Rev. Lett.* **91**, 147901 (2004).
- [10] A. Palevski, M. Heiblum, C. P. Umbach, C. M. Knoedler, A. Broers, and R. H. Koch, *Phys. Rev. Lett.* **62**, 1776 (1989).
- [11] H. Kosaka, T. Kawashima, A. Tomita, M. Notomi, T. Tamamura, T. Sato, and S. Kawakami, *Appl. Phys. Lett.* **74**, 1212 (1999).
- [12] L. Wu, M. Mazilu, and T. F. Krauss, *J. Lightwave Technol.* **21**, 561 (2003).
- [13] *The Quantum Hall Effect*, edited by R. E. Prange and S. M. Girvin (Springer, New York, 1987).
- [14] P. T. Rakich, M. S. Dahlem, S. Tandon, M. Ibanescu, M. Soljacic, G. S. Petrich, J. D. Joannopoulos, L. A. Kolodziejski, and E. P. Ippen, *Nature Mat.* **5**, 93 (2006).
- [15] J. D. Joannopoulos, S. G. Johnson, J. N. Winn, and

R. D. Meade, *Photonic Crystals: Molding the Flow of Light* (Princeton University Press, Princeton, New Jersey, USA, 2008).

- [16] K. S. Novoselov, A. K. Geim, S. V. Morozov, D. Jiang, M. I. Katsnelson, I. V. Grigorieva, S. V. Dubonos, and A. A. Firsov, *Nature* **438**, 197 (2005).
- [17] Y. Zhang, J. W. Tan, H. L. Stormer, and P. Kim, *Nature* **438**, 201 (2005).
- [18] C. Berger, Z. Song, X. Li, X. Wu, N. Brown, P. N. First, and W. A. de Heer, *Science* **312**, 1191 (2006).
- [19] F. Shedin, A. K. Geim, S. V. Morozov, E. W. Hill, P. Blake, M. I. Katsnelson, and K. S. Novoselov, *Nat. Mater.* **6**, 652 (2007).
- [20] K. I. Bolotin, K. J. Sikes, Z. Jiang, M. Klima, G. Fudenberg, J. Hone, P. Kim, and H. L. Stormer, *Solid State Commun.* **146**, 351 (2008).
- [21] M. I. Katsnelson, K. S. Novoselov, and A. K. Geim, *Nature Phys.* **2**, 620 (2006).
- [22] V. V. Chelano, V. Fal'ko, and B. L. Altshuler, *Science* **315**, 1252 (2007).
- [23] T. Ando, *J. Phys. Soc. Jpn.* **74**, 777 (2005).
- [24] P. L. McEuen, M. Bockrath, D. H. Cobden, Y.-G. Yoon, and S. G. Louie, *Phys. Rev. Lett.* **83**, 5098 (1999).
- [25] C.-H. Park, L. Yang, Y.-W. Son, M. L. Cohen, and S. G. Louie, *Nature Phys.* **4**, 213 (2008).
- [26] J. C. Meyer, C. O. Girit, M. F. Crommie, and A. Zettl, *Appl. Phys. Lett.* **92**, 123110 (2008).
- [27] S. Marchini, S. Günther, and J. Wintterlin, *Phys. Rev. B* **76**, 075429 (2007).
- [28] A. L. Vazquez de Parga, F. Calleja, B. Borca, M. C. G. P. Jr, J. J. Hinarejo, F. Guinea, and R. Miranda, *Phys. Rev. Lett.* **100**, 056807 (2008).
- [29] Y. Pan, N. Jiang, J. Sun, D. Shi, S. Du, F. Liu, and H.-J. Gao, <http://arxiv.org/abs/0709.2858> (2007).
- [30] J. B. Pendry and D. R. Smith, *Sci. Am.* **295**, 60 (2006).
- [31] T. Ando and T. Nakanishi, *J. Phys. Soc. Jpn.* **67**, 1704 (1998).
- [32] Talyanskii, V. I., Novikov, D. S., Simons, B. D., and L. S. Levitov, *Phys. Rev. Lett.* **87**, 276802 (2001).
- [33] D. S. Novikov, *Phys. Rev. B* **72**, 235428 (2005).

## Supporting Online Material: Analytical solution of electronic states of special graphene superlattices

When graphene is in a 1D external periodic potential  $V(x)$ , the Hamiltonian for electrons whose wavevectors are close to the  $\mathbf{K}$  point reads

$$H = \hbar v_0 (-i\sigma_x \partial_x + \sigma_y k_y + I V(x)/\hbar v_0), \quad (6)$$

where  $I$  is the  $2 \times 2$  identity matrix. In this case, we assume that the potential varies much more slowly than the carbon-carbon distance. So, the inter-valley scattering can be neglected safely [24, 31].

If a transform  $H' = U^\dagger H U$  is applied to Eq. (6) with the unitary matrix  $U = \exp(-i\sigma_x \alpha(x)/2)$ , where  $\alpha(x) = 2 \int_0^x V(x') dx' / \hbar v_0$  (we assume that a constant is subtracted from  $V(x)$  to set its average to zero), the resulting Hamiltonian  $H'$  reads

$$H' = \hbar v_0 (-i\sigma_x \partial_x + (\cos \alpha(x) \sigma_y - \sin \alpha(x) \sigma_z) k_y). \quad (7)$$

(A similar transform was applied to the Hamiltonian of a carbon nanotube under a sinusoidal potential for the specific case of finding the band gap opening behavior at the supercell Brillouin zone boundary [32, 33].) The terms having  $k_y$  could be treated as a perturbation if  $k_y$  is small. The eigenstate of the unperturbed Hamiltonian is given by

$$\psi'_{0s,\mathbf{k}}(\mathbf{r}) = \frac{1}{\sqrt{2}} \begin{pmatrix} 1 \\ s \operatorname{sgn}(k_x) \end{pmatrix} e^{i\mathbf{k} \cdot \mathbf{r}}. \quad (8)$$

Within second order perturbation theory, using Eqs. (7) and (8), the energy eigenvalue of the superlattice is

$$E_{s,\mathbf{k}} = s \hbar v_0 |k_x| + \hbar v_0 k_y^2 \sum_{s',\mathbf{G}} \frac{\left| \langle \psi'_{0s',\mathbf{k}+\mathbf{G}} | \cos \alpha(x) \sigma_y - \sin \alpha(x) \sigma_z | \psi'_{0s,\mathbf{k}} \rangle \right|^2}{s|k_x| - s'|k_x + G_x|}, \quad (9)$$

and the wavefunction is

$$\psi'_{s,\mathbf{k}}(\mathbf{r}) = \psi'_{0s,\mathbf{k}}(\mathbf{r}) + k_y \sum_{s',\mathbf{G}} \frac{\langle \psi'_{0s',\mathbf{k}+\mathbf{G}} | \cos \alpha(x) \sigma_y - \sin \alpha(x) \sigma_z | \psi'_{0s,\mathbf{k}} \rangle}{s|k_x| - s'|k_x + G_x|} \psi'_{0s,\mathbf{k}+\mathbf{G}}(\mathbf{r}). \quad (10)$$

Here,  $\mathbf{G}$ 's are the superlattice reciprocal lattice vectors

$\mathbf{G} = m \mathbf{G}_0$ , where  $\mathbf{G}_0 = (2\pi/L, 0)$  and  $m$  is an integer.

Therefore, in order for the superlattice to be an SGS, in which there is negligible dispersion with respect to  $k_y$ , the energy shift arising from the perturbation (or  $k_y$ ) should be negligible. Assuming that  $\mathbf{k}$  is small, the dominant summand is the case when  $s' = -s$  and  $m = 0$ . Thus, if

$$\langle \psi'_{-s,\mathbf{k}} | \cos \alpha(x) \sigma_y - \sin \alpha(x) \sigma_z | \psi'_{s,\mathbf{k}} \rangle = 0, \quad (11)$$

the superlattice would be an SGS. Under this condition, the relative deviation of the energy dispersion relation,

Eq. (9), from  $E_s(\mathbf{k}) = s\hbar v_0 |k_x|$  (Eq. (3) in the paper) is  $O(k_y^2/k_x G_x)$  and that of the wavefunction, Eq. (10), from Eq. (8) is  $O(k_y/G_x)$ . Similar quantities in a normal graphene superlattice are  $O(k_y^2/k_x^2)$  and  $O(k_y/k_x)$ , respectively. The eigenfunction  $\psi_{s,\mathbf{k}}(\mathbf{r})$  of the Hamiltonian  $H$  in Eq. (6) is, to a good approximation, obtained by  $\psi_{s,\mathbf{k}}(\mathbf{r}) = U\psi'_{0s,\mathbf{k}}(\mathbf{r})$  and is still an eigenstate of  $\sigma_x$  because  $U$  commutes with  $\sigma_x$ .